ЖЭТФ, 2012, том 142, вып. 6 (12), стр. 1309–1323

QUANTUM MAGNETO-OPTICS OF THE GRAPHITE FAMILY

L. A. Falkovsky *

Landau Institute for Theoretical Physics
119334, Moscow, Russia

Vereshchagin Institute of High Pressure Physics
142190, Troitsk, Moscow Region, Russia

Received May 29, 2012

The optical conductivity of graphene, bilayer graphene, and graphite in quantizing magnetic fields is studied. Both dynamical conductivities, longitudinal and Hall's, are evaluated analytically. The conductivity peaks are explained in terms of electron transitions. Correspondences between the transition frequencies and the magneto-optical features are established using the theoretical results. We show that trigonal warping can be considered within the perturbation theory for strong magnetic fields larger than 1 T. The semiclassical approach is applied for weak fields when the Fermi energy is much larger than the cyclotron frequency. The main optical transitions obey the selection rule with $\Delta n = 1$ for the Landau number n, but the $\Delta n = 2$ transitions due to the trigonal warping are also possible. The Faraday/Kerr rotation and light transmission/reflection in quantizing magnetic fields are calculated. Parameters of the Slonczewski–Weiss–McClure model are used in the fit taking the previous de Haas–van Alphen measurements into account and correcting some of them in the case of strong magnetic fields.

Contents

1. INTRODUCTION

Comprehensive literature on the graphene family can be described in terms of the Dirac gapless fermions. According to this picture, there are two bands at the K hexagon vertexes of the Brillouin zone without any gap between them, and the electron dispersion can be considered linear in a wide wavevector region. For the dispersion linearity, this region should be small compared with the size of the Brillouin zone, i. e., less than 10^8 cm^{-1}, providing the small carrier concentration $n \ll 10^{16}$ cm^{-2}. Pristine graphene at zero temperature has no carriers, and the Fermi level should separate the conduction and valence bands. However, undoped graphene cannot be really obtained, and the purest graphene so far contains about $n \sim 10^9$ cm^{-2} carriers. Then the following problem appears: how do Coulomb electron–electron interactions renormalize the linear dispersion and does graphene become an insulator with a gap?

*E-mail: falk@itp.ac.ru

Semiconductors with a gap are needed for electronic applications. Investigations of the graphene bilayer and multilayer are very popular because the gap appears when the bias is applied. We see how physics made a circle over half a century, returning to graphite studies. Slonczewski, Weiss, and McClure (SWMC) should be mentioned here because they have stated the description of a layered matter [1] with interactions that are strong in the layer and weak between layers.

The most accurate investigation of the band structure of metals and semiconductors is a study of the Landau levels through experiments such as magneto-optics [2–10] and magneto-transport [11–15]. In magnetic fields, the classical and quantum Hall effects are observed, as is the polarization rotation for transmitted light (the Faraday rotation) or reflected light (the Kerr rotation). However, the interpretation of the experimental results involves a significant degree of uncertainty, because it is not clear how the resonances can be identified and which electron transitions they correspond to.

The theoretical solution of the band problem in magnetic fields often cannot be found exactly. A typical example is presented by graphene layers. For bilayer graphene and graphite, the effective Hamiltonian is a 4×4 matrix giving four energy bands. The trigonal warping described by the effective Hamiltonian with a relatively small parameter γ_3 provides an evident effect. Another important parameter is the gate-tunable bandgap U in bilayer graphene. In this situation, the quantization problem cannot be solved within a rigorous method. To overcome this difficulty, several methods have been proposed for approximate [9, 16–19], numerical [20–24], and semiclassical quantization [25, 26].

This paper is organized as follows. In Sec. 2, we recall the electron dispersion in graphene, bilayer graphene, and graphite. In Sec. 3, the optical conductivity and light transmission are discussed. In Secs. 4 and 5, we describe the quantization in magnetic fields in detail. In Sec. 6, the longitudinal and Hall conductivities and the Faraday/Kerr rotation are described.

2. ELECTRON DISPERSION IN THE GRAPHENE FAMILY

2.1. Electron dispersion in graphene

The symmetry of the K point is C_{3v} with a threefold axis and reflection planes. This group has a twofold representation with the basis functions transforming one into another under reflections and acquiring the factors $\exp(\pm 2\pi i/3)$ under rotations. The linear momentum variations from the K point, $p_\pm = \mp i p_x - p_y$, transform similarly. The effective Hamiltonian is invariant under the group transformations, and we have a unique possibility to construct the invariant Hamiltonian linear in the momentum as

$$H(\mathbf{p}) = \begin{pmatrix} 0 & vp_+ \\ vp_- & 0 \end{pmatrix}, \tag{1}$$

where v is a constant of the dimension of velocity. The same Hamiltonian has been written using the tight-binding model.

The eigenvalues of this matrix give two bands,

$$\varepsilon_{1,2} = \mp v\sqrt{p_x^2 + p_y^2} = \mp vp,$$

where the sign "$\mp$" corresponds to holes and electrons. The gapless linear spectrum arises as a consequence of the symmetry, and the chemical potential at zero temperatures coincides with the band crossing due to the carbon valence. The cyclotron mass is given by

$$m(\varepsilon) = \frac{1}{2\pi}\frac{dS(\varepsilon)}{d\varepsilon} = \frac{\varepsilon}{v^2},$$

and the carrier concentration at zero temperature $n(\mu) = \mu^2/\pi\hbar^2 v^2$ is expressed in terms of the chemical potential μ.

By tuning the gate voltage, the linearity of the spectrum has been examined in the Shubnikov–de Haas studies [27] with the help of the relation $m(\mu)v = \mp\hbar\sqrt{\pi n(\mu)}$ between the effective mass and the carrier concentration at the Fermi level. The "constant" parameter v was found to be no longer constant; at low carrier concentrations $n \sim 10^9$ cm^{-2}, it exceeds its usual value $v = (1.05 \pm 0.10) \cdot 10^8$ cm/s (at concentrations $n > 10^{11}$ cm^{-2}) by a factor of 3.

This is a result of electron–electron interactions, which become stronger at low carrier concentrations. The logarithmic renormalization of the velocity was found by Abrikosov and Beneslavsky in Ref. [28] for the three-dimensional case and in Refs. [29, 30] for two-dimensional graphene. We note that no phase transition was revealed even at the lowest carrier concentration. We can conclude that the Coulomb interactions do not create any gap in the spectrum.

2.2. Electron dispersion in bilayer graphene and graphite

Bilayer graphene has attracted much interest partly due to the opening of a tunable gap in its electronic

Table. The parameters of the Hamiltonian, Eq. (2), their values in the SWMC model, and the values obtained in experimental works, all in meV

Eq. (2)	γ_0 3050	γ_1 360	γ_2 -10.2	γ_3 270	γ_4 -150	γ_5 -1.5	Δ 16	ε_F -4.1
S[a]	γ_0	γ_1	$2\gamma_2$	γ_3	$-\gamma_4$	$2\gamma_5$	$\Delta + 2(\gamma_2 - \gamma_5)$	$2\gamma_2 + \varepsilon_F$
M[b]	3160	390	-20	276	44	38	8	-24
D[c]	3120	380	-21	315	120	-3	-2	–
DFT[d]	2598±15	364±20	-14 ± 8	319±20	177±25	36±13	24±10	-13 ± 8

[a]SWMC [1], [b]Mendez et al. [5], [c]Doezema et al. [4], [d]Charlier et al. [41].

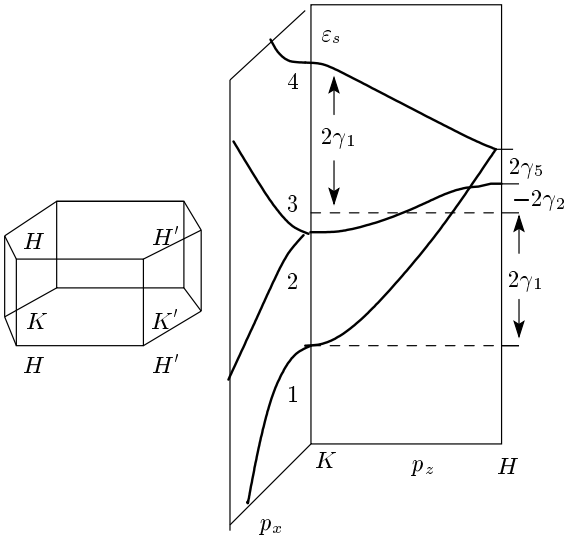

Fig. 1. Band structure of graphite

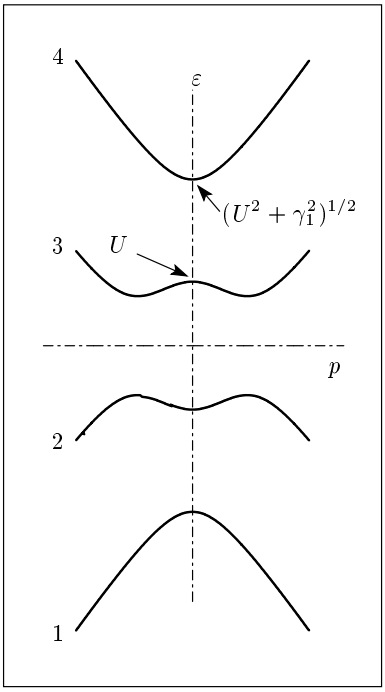

Fig. 2. Band structure of bilayer graphene

spectrum by an external electrostatic field. Such a phenomenon was predicted in Refs. [31, 32] and was observed in optical studies controlled by applying a gate voltage [33–40].

The effective Hamiltonian of the SWMC theory can be written [22, 23] near the KH line in graphite as

$$H(\mathbf{p}) = \begin{pmatrix} \tilde{\gamma}_5 & vp_+ & \tilde{\gamma}_1 & \dfrac{\tilde{\gamma}_4 v p_-}{\gamma_0} \\ vp_- & \tilde{\gamma}_2 & \dfrac{\tilde{\gamma}_4 v p_-}{\gamma_0} & \dfrac{\tilde{\gamma}_3 v p_+}{\gamma_0} \\ \tilde{\gamma}_1 & \dfrac{\tilde{\gamma}_4 v p_+}{\gamma_0} & \tilde{\gamma}_5 & vp_- \\ \dfrac{\tilde{\gamma}_4 v p_+}{\gamma_0} & \dfrac{\tilde{\gamma}_3 v p_-}{\gamma_0} & vp_+ & \tilde{\gamma}_2 \end{pmatrix}, \quad (2)$$

where $p_\pm = \mp i p_x - p_y$ are the momentum components and $\tilde{\gamma}_j$ are the functions of the p_z momentum in the major axis direction,

$$\tilde{\gamma_2} = 2\gamma_2 \cos(2p_z d_0), \quad \tilde{\gamma}_5 = 2\gamma_5 \cos(2p_z d_0) + \Delta,$$

$$\tilde{\gamma}_i = 2\gamma_i \cos(p_z d_0), \quad i = 1, 3, 4,$$

with the distance $d_0 = 3.35$ Å between layers in graphite. The nearest-neighbor hopping integral $\gamma_0 \approx \approx 3$ eV corresponds with the velocity parameter $v = = 1.5 a_0 \gamma_0 = 10^6$ m/s and the in-layer inter atomic distance $a_0 = 1.415$ Å. Hamiltonian (2) is represented in a somewhat different form than in Ref. [1]. The relations between the hopping integrals in these forms are given in the Table. The recent estimate [35, 36] of the parameters agrees with those given in the Table.

The electron spectrum of graphite is shown in Fig. 1. There are four levels labeled by $s = 1, 2, 3, 4$ from below at any momentum. As a consequence of the axial symmetry, a twofold degeneration $\varepsilon_2 = \varepsilon_3$ exists at $p_x = p_y = 0$, i. e., on the KH line.

In bilayer graphene, every layer has only one neighboring layer. Therefore, we have to set $\gamma_2 = \gamma_5 = 0$ and to substitute $\tilde{\gamma}_i = \gamma_i$ for $i = 1, 3, 4$ in Hamiltonian (2). The parameter U can also be included in the bilayer Hamiltonian as a result of the gate voltage. Then the gap appears between ε_2 and ε_3, and these bands acquire the shape of a "mexican hat" (Fig. 2). Importantly, two points, K and K', are in the Brillouin zone and transforming one into another under reflection. Such a reflection changes the U sign, giving two different dispersion laws at the K and K' points.

3. OPTICAL CONDUCTIVITY

We use the general expression for the conductivity as a function of the electric field frequency ω and wave vector k in the form [42, 43]

$$\sigma_{ij}(\omega,k) = 2ie^2 \sum_{\mathbf{p},m>n} \left\{ \frac{v^i_{mm} v^j_{mm} \{f_0[\varepsilon_m(\mathbf{p}_-)] - f_0[\varepsilon_m(\mathbf{p}_+)]\}}{[\varepsilon_m(\mathbf{p}_+) - \varepsilon_m(\mathbf{p}_-)][\omega - \varepsilon_m(\mathbf{p}_+) + \varepsilon_m(\mathbf{p}_-)]} + \right.$$
$$\left. + \frac{2\omega v^i_{mn} v^j_{nm} \{f_0[\varepsilon_m(\mathbf{p}_-)] - f_0[\varepsilon_n(\mathbf{p}_+)]\}}{[\varepsilon_n(\mathbf{p}_+) - \varepsilon_m(\mathbf{p}_-)]\{(\omega+i\delta)^2 - [\varepsilon_n(\mathbf{p}_+) - \varepsilon_m(\mathbf{p}_-)]^2\}} \right\}, \quad (3)$$

valid in the collisionless limit $(\omega, kv) \gg \tau^{-1}$, where τ^{-1} is the electron relaxation frequency, $\mathbf{p}_\pm = \mathbf{p} \pm \mathbf{k}/2$, and v^i_{mn} is the matrix element of the velocity operator

$$\mathbf{v} = \frac{\partial H(\mathbf{p})}{\partial \mathbf{p}} \quad (4)$$

determined by Hamiltonian (1) or (2). Hitherto, we did not use any peculiarities of the graphene spectrum. The expression acquired only the factor 4 due to summation over spin and over six points of the K type (two per a Brillouin zone).

The first term in Eq. (3) corresponds to the intraband electron–photon scattering processes. In the limit of the high carrier concentration $(T, E_F) \gg kv$, it coincides with the usual Drude–Boltzmann conductivity if the substitution $\omega \to \omega + i\tau^{-1}$ is made. The second term owes its origin to the interband $n \to m$ transitions with the infinitesimal δ determining a bypass around the pole in integrating over the momentum $\mathbf{p}$. The real part of this contribution reduces to the well-known expression for the absorbed energy due to direct interband transitions.

Optical conductivity of graphene

For optical frequencies $\omega \gg kv$, we can integrate over the angle in Eq. (3) and write the conductivity as

$$\sigma(\omega) = \frac{e^2\omega}{i\pi\hbar} \left[\int_{-\infty}^{\infty} d\varepsilon \frac{|\varepsilon|}{\omega^2} \frac{df(\varepsilon)}{d\varepsilon} - \right.$$
$$\left. - \int_0^{\infty} d\varepsilon \frac{f(-\varepsilon) - f(\varepsilon)}{(\omega+i\delta)^2 - 4\varepsilon^2} \right] \quad (5)$$

using the variable $\varepsilon = vp$.

The intraband term can be integrated once more,

$$\sigma^{intra}(\omega) = \frac{2ie^2T}{\pi\hbar(\omega + i\tau^{-1})} \ln\left(2 \operatorname{ch} \frac{\mu}{2T}\right), \quad (6)$$

where we write $\omega + i\tau^{-1}$ instead of ω to take the small relaxation frequency into account. This Drude–Boltzmann conductivity at low temperatures $T \ll \mu$ takes the form

$$\sigma^{intra}(\omega) = \frac{ie^2|\mu|}{\pi\hbar(\omega + i\tau^{-1})}$$

In the opposite limit of high temperatures, the intraband conductivity (6) becomes

$$\sigma^{intra}(\omega) = \frac{2ie^2T\ln 2}{\pi\hbar(\omega + i\tau^{-1})}.$$

The temperature dependence of the relaxation rate in graphene is discussed theoretically in Ref. [44].

The interband contribution in Eq. (5) integrated at zero temperatures gives

$$\sigma^{inter}(\omega) = \frac{e^2}{4\hbar} \left[\theta(\omega - 2\mu) - \frac{i}{2\pi} \ln \frac{(\omega+2\mu)^2}{(\omega-2\mu)^2} \right],$$

where the θ-function expresses the threshold behavior of interband electron transitions at $\omega = 2\mu$. The temperature smooths out all the singularities:

$$\theta(\omega - 2\mu) \to \frac{1}{2} + \frac{1}{\pi} \operatorname{arctg} \frac{\omega - 2\mu}{2T},$$
$$(\omega - 2\mu)^2 \to (\omega - 2\mu)^2 + (2T)^2.$$

The main issue should be emphasized. In the high-frequency region $\omega \gg (T, \mu)$, the interband transitions make the main contribution to the conductivity

$$\sigma(\omega) = \frac{e^2}{4\hbar},$$

which has a universal character independent of any material parameters. This frequency region is bounded above by the band width of around 3 eV. Using the universal conductivity, we can calculate the light transmission through graphene [45] in the approximation linear in conductivity,

$$T = 1 - \frac{4\pi}{c}\,\mathrm{Re}\,\sigma(\omega)\cos\theta = 1 - \pi\frac{e^2}{\hbar c}\cos\theta,$$

where θ is the incidence angle. The intensity of reflected light is quadratic in the fine structure constant $\alpha = e^2/\hbar c$. In excellent agreement with the theory, for a wide optical range, several experimental groups [46–48] observe light transmission through graphene as well as bilayer graphene where the difference from unity is twice as large. It is exceptionally intriguing that light transmission involves the fine structure constant of quantum electrodynamics, having really no relation to the graphene physics.

For graphite, the value $\sigma_d = e^2/4\hbar d_0$ plays the role of a universal dynamical conductivity, where d_0 is the distance between layers. As is shown experimentally [49] and theoretically [50], the dynamical conductivity of graphite is close to this universal value in the frequency range 0.1–1 eV, having the kink singularity at the interband transition frequency $\omega = 2\gamma_1$.

4. GRAPHENE IN MAGNETIC FIELDS

In the presence of a magnetic field B, the momentum projections p_+ and p_- become operators with the commutation rule $\{\hat{p}_+, \hat{p}_-\} = -2e\hbar B/c$. We use the relations

$$v\hat{p}_+ = \omega_B a, \quad v\hat{p}_- = \omega_B a^\dagger$$

involving the creation ($a^\dagger$) and annihilation (a) operators with $\omega_B = v\sqrt{2|e|\hbar B/c}$. We write only one of the two xy space coordinates including the corresponding degeneracy proportional to the magnetic field in the final results.

For graphene, we seek the eigenfunction of Hamiltonian (1) in the form [51, 52]

$$\psi^{\alpha}_{sn}(x) = \begin{cases} C^1_{sn}\varphi_{n-1}(x) \\ C^2_{sn}\varphi_n(x) \end{cases}, \qquad (7)$$

where $\varphi_n(x)$ are orthonormal Hermite functions with the Landau number $n \geq 0$. Eliminating the Hermite functions from the equations, we obtain a system of linear equations for the eigenvector $\mathbf{C}_{sn}$,

$$\begin{pmatrix} -\varepsilon & \omega_B\sqrt{n} \\ \omega_B\sqrt{n} & -\varepsilon \end{pmatrix} \times \begin{cases} C^1_{sn} \\ C^2_{sn} \end{cases} = 0,$$

which gives the eigenvalues

$$\varepsilon_{sn} = \mp\omega_B\sqrt{n} \qquad (8)$$

with $s = 1, 2$ and $n = 0, 1, 2, \ldots$ For $n = 0$, there is only one level $\varepsilon_{10} = 0$ with $C^1_0 = 0$ and $C^2_0 = 1$, as follows from Eq. (7). The wave function columns are

$$\begin{matrix} C^1_{sn} \\ C^2_{sn} \end{matrix} = \frac{1}{\sqrt{2}} \begin{cases} 1 \\ -1 \end{cases} \quad \text{and} \quad \begin{matrix} 1 \\ 1 \end{matrix}$$

for $s = 1$ and $s = 2$ and $n = 1, 2, \ldots$

5. GRAPHENE LAYERS WITH TRIGONAL WARPING IN MAGNETIC FIELDS

We seek eigenfunction of Hamiltonian (2) as a column

$$\psi^{\alpha}_{sn}(x) = \begin{cases} C^1_{sn}\varphi_{n-1}(x) \\ C^2_{sn}\varphi_n(x) \\ C^3_{sn}\varphi_{n-1}(x) \\ C^4_{sn}\varphi_{n-2}(x) \end{cases}. \qquad (9)$$

We see the every row in Hamiltonian (2) becomes proportional to a definite Hermite function if the terms with γ_3 are omitted. We show that the terms proportional to γ_3/γ_0 can be considered within the perturbation theory or the semiclassical approximation.

Eliminating the Hermite functions from the equations, we obtain a system of linear equations for the eigenvector $\mathbf{C}_{sn}$,

$$\begin{pmatrix} \tilde{\gamma}_5 - \varepsilon & \omega_B\sqrt{n} & \tilde{\gamma}_1 & \omega_4\sqrt{n-1} \\ \omega_B\sqrt{n} & \tilde{\gamma}_2 - \varepsilon & \omega_4\sqrt{n} & 0 \\ \tilde{\gamma}_1 & \omega_4\sqrt{n} & \tilde{\gamma}_5 - \varepsilon & \omega_B\sqrt{n-1} \\ \omega_4\sqrt{n-1} & 0 & \omega_B\sqrt{n-1} & \tilde{\gamma}_2 - \varepsilon \end{pmatrix} \times \begin{cases} C^1_{sn} \\ C^2_{sn} \\ C^3_{sn} \\ C^4_{sn} \end{cases} = 0\,, \qquad (10)$$

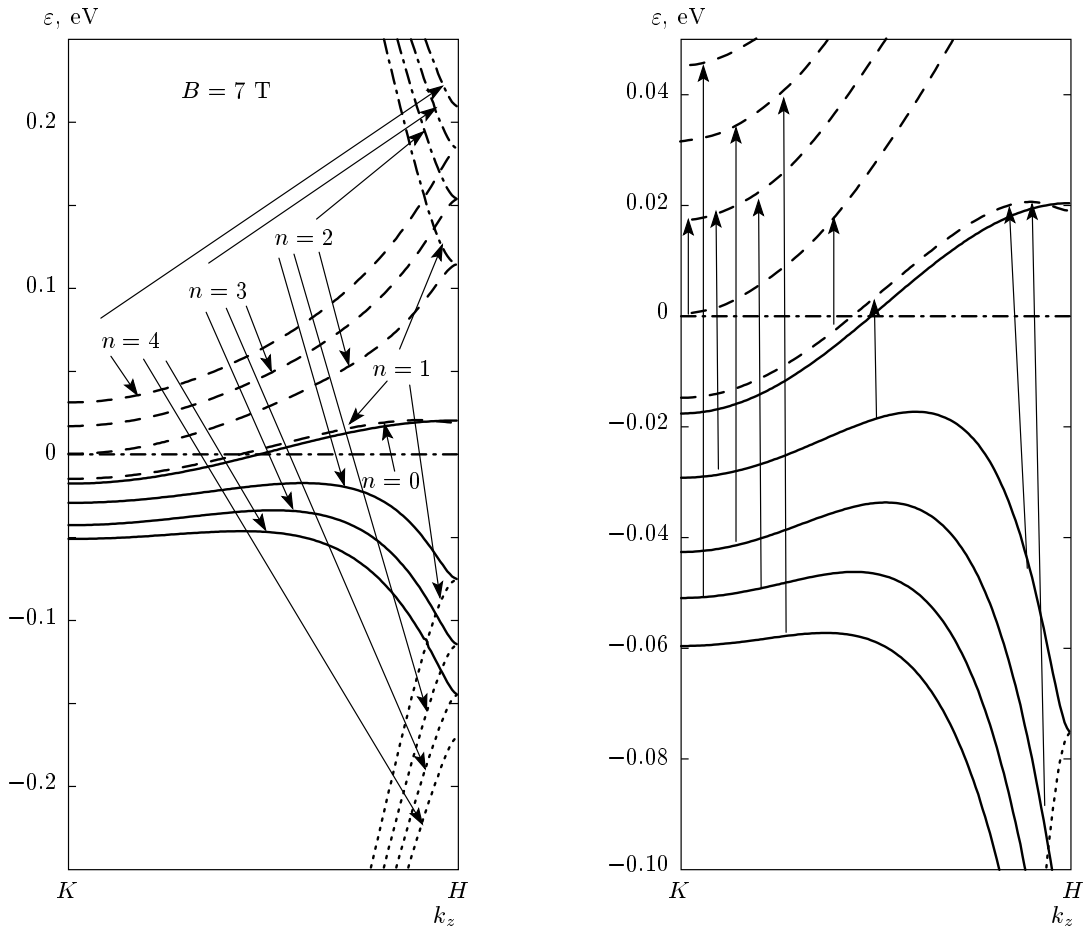

Fig. 3. Landau levels in graphite ε_{sn} for n from 0 to 4 in four bands $s = 1, 2, 3$, and 4 (in dotted, solid, dashed, and dash-dotted lines, correspondingly) as functions of the wave vector k_z along the KH line in the Brillouin zone ($K = 0$, $H = \pi/2d_0$) in the magnetic field $B = 7$ T with the SWMC model parameters given in the Table. The main electron transitions shown in the right panel below 100 meV occur between the levels with the selection rule $\Delta n = 1$

where the band number $s = 1, 2, 3, 4$ labels the solutions at a given n from the bottom, $\omega_B = v\sqrt{2|e|\hbar B/c}$, and $\omega_4 = \tilde{\gamma}_4\omega_B/\gamma_0$.

The eigenvalues of the matrix in Eq. (10) are easy to find; they are shown in Fig. 3 as functions of the momentum p_z. For each Landau number $n \geq 2$ and momentum p_z, there are four eigenvalues $\varepsilon_s(n)$ and four corresponding eigenvectors, Eq. (9), labeled by the band subscript s. We use the notation $|sn\rangle$ for levels. In addition, there are four levels. One of them is

$$\varepsilon_1(n = 0) = \tilde{\gamma}_2 \tag{11}$$

for $n = 0$ with the eigenvector $\mathbf{C}_0 = (0, 1, 0, 0)$, as is evident from Eq. (9). This level intersects the Fermi level and belongs to the electron (hole) band near the K (H) point. The other three levels labeled by $n = 1$ and $s = 1, 2, 3$ are determined by the first three equations of system (10) with $C^4_{s1} = 0$.

The $|21\rangle$ level is close to the $|10\rangle$ level. In the region p_z, $\gamma_1/\cos(2p_zd_0) \gg \gamma_2$, where the electrons are located, this level has the energy

$$\varepsilon_2(n = 1) = \tilde{\gamma}_2 - 2\frac{\omega_B^2\tilde{\gamma}_4}{\tilde{\gamma}_1\gamma_0}.$$

In the same region, the two closest bands ($s = 2, 3$) with $n \geq 2$ are written as

$$\varepsilon_{2,3}(n) = \tilde{\gamma}_2 - \frac{\omega_B^2\tilde{\gamma}_4}{\tilde{\gamma}_1\gamma_0}(2n-1) \mp \frac{\omega_B^2}{\tilde{\gamma}_1}\sqrt{n(n-1)} \tag{12}$$

with the accuracy of $(\tilde{\gamma}_4/\gamma_0)^2$.

5.1. Perturbation theory for the matrix Hamiltonian

Due to the double degeneracy existing on the KH line, the effect of trigonal warping becomes essential. The simplest way to evaluate the corrections resulting from the warping γ_3 is to consider the Green's function having the poles at the electron levels.

The Green's function of the unperturbed Hamiltonian is given by

$$G_0^{\alpha\beta}(\varepsilon, x, x') = \sum_{sn} \frac{\psi_{sn}^{\alpha}(x)\psi_{sn}^{*\beta}(x')}{\varepsilon - \varepsilon_{sn}}, \qquad (13)$$

which involves the functions in Eq. (9). The corrections to the levels can be found by iterations,

$$\mathbf{G}_{m+1}(x, x') = \int d^2x'' \mathbf{G}_0(x, x'')\mathbf{V}(x'')\mathbf{G}_m(x'', x'),$$

where $\mathbf{V}(\mathbf{x})$ has only two matrix elements $V^{42} = \omega_B\tilde{\gamma}_3 a^+/\gamma_0$ and $V^{24} = V^{42*}$ in Hamiltonian (2).

At the second iteration, we obtain the corrections

$$\int d^2x_1 d^2x_2 G_0^{\alpha 4}(x, x_1)V^{42}(x_1)G_0^{22}(x_1, x_2) \times \times V^{24}(x_2)G_0^{4\beta}(x_2, x')$$

and a similar term with the superscript substitution $2 \leftrightarrow 4$. The matrix elements of the perturbation V are easily calculated with respect to the Hermite functions in Eqs. (13) and (9), and we obtain

$$\left(\frac{\omega_B\tilde{\gamma}_3}{\gamma_0}\right)^2 \times \times \sum_{s'sn} \frac{(n-2)|C_{sn}^4 C_{s',n-3}^2|^2 \psi_{sn}^{\alpha}(x)\psi_{sn}^{*\beta}(x')}{(\varepsilon - \varepsilon_{sn})(\varepsilon - \varepsilon_{s',n-3})(\varepsilon - \varepsilon_{sn})}, \qquad (14)$$

for the diagram shown in the upper part of Fig. 4. This correction plays an important role near the poles of the Green's function. For this reason, for ε close to ε_{sn}, the ε value in the second factor of the denominator can be replaced by ε_{sn}. Thus, the total Green's function (with the correction) has the structure

$$\frac{1}{\varepsilon - \varepsilon_{sn}} + \frac{\delta}{(\varepsilon - \varepsilon_{sn})^2},$$

which can be rewritten up to second-order terms in δ as

$$\frac{1}{\varepsilon - \varepsilon_{sn} - \delta}.$$

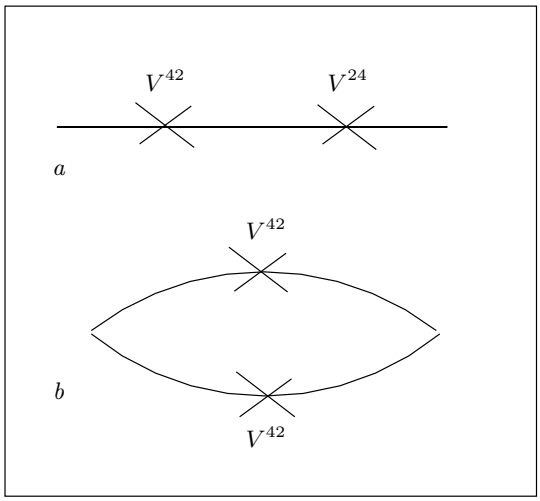

Fig. 4. Diagrams for the second iteration of the perturbation theory; (a) corrections to the Green's function, (b) corrections to the vertex in conductivity

Therefore, we can represent [16] the correction as a shift $\delta\varepsilon_{sn}$ of the poles $(\varepsilon - \varepsilon_{sn} - \delta\varepsilon_{sn})^{-1}$ with

$$\delta\varepsilon_s(n) = \left(\frac{\omega_B\tilde{\gamma}_3}{\gamma_0}\right)^2 \sum_{s'} \left\{ \frac{(n-2)|C_{sn}^4 C_{s',n-3}^2|^2}{\varepsilon_s(n) - \varepsilon_{s'}(n-3)} + \right. \left. + \frac{(n+1)|C_{sn}^2 C_{s',n+3}^4|^2}{\varepsilon_s(n) - \varepsilon_{s'}(n+3)} \right\}, \qquad (15)$$

where the first term should be omitted for $n - 3 < 0$. In fact, our illustration is nothing but a calculation of the electron self-energy and the naive expansion of the denominator can indeed be replaced by summing the corresponding diagrams.

The corrected $|10\rangle$ level is given by

$$\varepsilon_1(n = 0) = \tilde{\gamma}_2 + \left(\frac{\omega_B\tilde{\gamma}_3}{\gamma_0}\right)^2 \sum_{s'} \frac{|C_{s'3}^4|^2}{\tilde{\gamma}_2 - \varepsilon_{s'}(3)}. \qquad (16)$$

The $|21\rangle$ level is very close to the level with $n = 0$, Eq. (16).

Comparing the corrections, Eq. (15), with the leading contribution in Eq. (12), we find, first, that the perturbation theory is valid when the expansion parameter $(\tilde{\gamma}_3\tilde{\gamma}_1/\gamma_0\omega_B)^2$ becomes small, i. e., for strong magnetic fields $B > 1$ T. Second, the effect of γ_4 is linear, whereas that of γ_3 is quadratic in these constants. Therefore, the γ_4 constant is more essential for the electron levels in magnetic fields.

Comparison shows that Eqs. (15) and (16) for levels give the same results as the numerical method of truncating the infinite-rank matrix in Ref. [21].

We note that the derived expressions are also applicable to bilayer graphene if we include the field U and set $\gamma_2 = \gamma_5 = 0$ and $\tilde{\gamma}_i = \gamma_i$ for $i = 1, 3, 4$. In the simplest approach, when only the main parameters γ_1 and U are retained, the magnetic levels ε_{sn} are determined by the equation

$$[(U-\varepsilon_{sn})^2 - \omega_B^2 n][(U+\varepsilon_{sn})^2 - \omega_B^2(n+1)] + \\ + \gamma_1^2(U^2 - \varepsilon_{sn}^2) = 0.$$

5.2. Berry phase, semiclassical quantization, and Landau levels

Alternatively, semiclassical quantization can be used for relatively weak magnetic fields when the cyclotron frequency is small compared with the Fermi energy. We can then use the Bohr–Sommerfeld condition in the form

$$\frac{c}{e\hbar B} S(\varepsilon) = 2\pi \left[n_{sc} + \frac{\mathcal{T}}{4} + \delta(\varepsilon) \right], \qquad (17)$$

where $S(\varepsilon)$ is the cross-sectional area of the electron orbit in the $p_x p_y$ space for the energy ε and the constant momentum projection p_z on the magnetic field, n_{sc} is an integer supposed to be large. The integer $\mathcal{T}$ is the number of smooth turning points on the electron orbit. There are two smooth turning points for the Landau levels and only one for skipping electrons reflected by the hard edge.

We use the semiclassical approach for the magnetic field normal to the layered system when only the in-layer momentum components p_x and p_y are quantized and the size of the Fermi surface is small compared with the Brillouin zone size. We note that the $\delta(\varepsilon)$ phase depends on the energy. If the spin is neglected, $\delta = 0$ and $\mathcal{T} = 2$ for the Landau levels, and $\delta = 1/2$ and $\mathcal{T} = 2$ for monolayer graphene. In these two cases, the semiclassical result coincides with the rigorous quantization and it is closely connected with the topological Berry phase [53]. This δ-phase was evaluated for bismuth in Ref. [25], preceding Berry's work by almost two decades, and it was considered again for bismuth in Ref. [54]. For graphite, semiclassical quantization was applied in Ref. [26]. However, in the general case, the evaluation of the δ-phase still attracts much interest [55–61].

The problem under consideration is described by the Hamiltonian in Eq. (1) or (2) rewritten in the form

$$(\mathbf{V} \cdot \tilde{\mathbf{p}} + \Gamma - \varepsilon)\Psi = 0, \qquad (18)$$

where $\tilde{\mathbf{p}}$ and $\mathbf{V}$ are the respective two-dimensional vector and matrix, with the in-layer components x and y. The column Ψ is labeled by the band subscript which we omit together with the matrix subscripts on Γ and $\mathbf{V}$, summation over them is implied in Eq. (18). The matrices Γ and $\mathbf{V}$ are the first two terms (of zero and first orders) in a series expansion of the Hamiltonian in powers of quasi-momenta p_x and p_y.

In the magnetic field, the momentum operator $\tilde{\mathbf{p}}$ depends on the vector potential $\mathbf{A}$ by means of the Peierls substitution,

$$\tilde{\mathbf{p}} = -i\hbar\nabla - e\mathbf{A}/c,$$

providing the gauge invariance of the theory. The magnetic field can also enter explicitly, describing the magnetic interaction with the spin of particles. However, for the graphene family, the magnetic interaction is weak and omitted here.

It is convenient to choose the vector potential in the Landau gauge $A_x = -By$, $A_y = A_z = 0$ in such a way that the Hamiltonian is independent of the x coordinate. We seek the function Ψ in the form

$$\Psi = \Phi \exp(is/\hbar),$$

where the function s is assumed to be common for all component of the column Ψ.

The function Φ is expanded in series in $\hbar/i$:

$$\Phi = \sum_{m=0}^{\infty} \left(\frac{\hbar}{i}\right)^m \varphi_m.$$

Collecting the terms with the same powers of $\hbar$ in Eq. (18), we have

$$(\mathbf{V} \cdot \mathbf{p} + \Gamma - \varepsilon)\varphi_m = -\mathbf{V}\nabla\varphi_{m-1}. \qquad (19)$$

For $m = 0$, we obtain a homogeneous system of algebraic equations for the wave function column φ_0,

$$(\mathbf{V} \cdot \mathbf{p} + \Gamma - \varepsilon)\varphi_0 = 0, \qquad (20)$$

which has a solution under the condition

$$\mathrm{Det}(\mathbf{V} \cdot \mathbf{p} + \Gamma - \varepsilon) = 0. \qquad (21)$$

This equation determines the classical electron orbit, $\varepsilon(p_x, p_y) = \varepsilon$, at a given electron energy ε in presence of the magnetic field. On the other hand, the equation coincides with the dispersion equation since it does not contain the magnetic field. In the three-dimensional case, as in graphite, the dispersion also depends on the momentum projection p_z on the magnetic field. Therefore, our scheme does not require the expansion in powers of p_z.

Equations (19) with $m = 0, 1$ give the wave function in the semiclassical approximation [25]. The quantization condition can be written, as usual, from the

requirement that the wave function be single valued. Making the bypass in the complex plane around the turning points to obtain decreasing solutions in the classically inaccessible region, we obtain, first, $\mathcal{T} = 2$ and, second, the δ-phase as a contour integral along the classical orbit

$$\delta(\varepsilon) = \frac{1}{2\pi}\mathrm{Im}\oint \frac{dp_x}{\varphi_0^*\varphi_0 v_y}\varphi_0^* V_y \frac{d\varphi_0}{dp_x}, \qquad (22)$$

where $v_y = \partial\varepsilon(p_x, p_y)/\partial p_y$. Using the Hamiltonian hermiticity, after the simple algebra (see Ref. [25]), Eq. (22) can be rewritten in the gauge-invariant form

$$\delta(\varepsilon) = \frac{1}{4\pi}\mathrm{Im}\oint \frac{dp}{\varphi_0^*\varphi_0 v}\varphi_0^*\left[\mathbf{V}\times\frac{d}{d\mathbf{p}}\right]_z\varphi_0, \qquad (23)$$

where $v = \sqrt{v_x^2 + v_y^2}$ and the integrand is called the Berry connection (or curvature). Everywhere, the summation over the band subscript is implied.

We emphasize that Eqs. (22) and (23) yield $|\delta(\varepsilon)| = 1/2$ for monolayer graphene, which, together with $\mathcal{T} = 2$, gives the same Landau levels as the exact quantization (8).

We now calculate the δ-phase for bilayer graphene. In the simplest case, omitting γ_3 and γ_4, the effective Hamiltonian can be written as

$$H(\mathbf{p}) = \begin{pmatrix} U & q_+ & \gamma_1 & 0 \\ q_- & U & 0 & 0 \\ \gamma_1 & 0 & -U & q_- \\ 0 & 0 & q_+ & -U \end{pmatrix}, \qquad (24)$$

where the parameter U describes the tunable gap due to the gate voltage and γ_1 is the interlayer nearest-neighbor hopping integral energy. The constant velocity parameter v is incorporated in the notation $q_\pm = vp_\pm$. The band structure is shown in Fig. 2. The minimal value of the upper energy ε_4 is $\sqrt{U^2+\gamma_1^2}$, and the ε_3 band takes the maximal value $|U|$ at $q = 0$. Here, the orbit is the circle defined by Eq. (21), written in the form

$$[(U+\varepsilon)^2 - q^2][(U-\varepsilon)^2 - q^2] - \gamma_1^2(\varepsilon^2 - U^2) = 0. \qquad (25)$$

The eigenfunction φ_0 of Hamiltonian (24) can be taken as

$$\varphi_0 = \begin{pmatrix} (U-\varepsilon)[(\varepsilon+U)^2 - q^2] \\ q_-[q^2 - (\varepsilon+U)^2] \\ \gamma_1(U^2 - \varepsilon^2) \\ \gamma_1 q_+(U-\varepsilon) \end{pmatrix}, \qquad (26)$$

with the norm squared

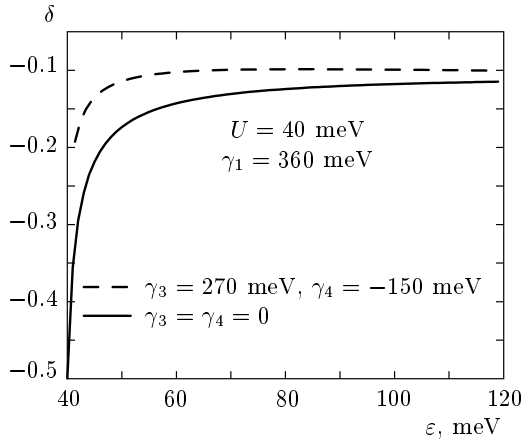

Fig. 5. Semiclassical phase vs energy in the conduction band of bilayer graphene without trigonal warping (solid line) and with the warping (dashed line)

$$\varphi_0^*\varphi_0 = [(\varepsilon+U)^2 - q^2]^2[(\varepsilon-U)^2 + q^2] + \\ + \gamma_1^2(\varepsilon-U)^2[(\varepsilon+U)^2 + q^2]. \qquad (27)$$

The derivatives for Eq. (22) are calculated along the trajectory where the energy ε and, consequently, the trajectory radius q are constant.

If the conditions $|U| < |\varepsilon| < \sqrt{U^2+\gamma_1^2}$ are fulfilled, Eq. (25) has only one solution for the radius squared

$$q^2 = U^2 + \varepsilon^2 + \sqrt{4U^2\varepsilon^2 + (\varepsilon^2 - U^2)\gamma_1^2}.$$

The matrix $V_y = \partial H/\partial p_y$ in Eq. (22) has four nonzero elements, $V_y^{12} = V_y^{21} = V_y^{34} = V_y^{43} = -1$.

Using Eqs. (25) and (26), we find

$$\mathrm{Im}\,\varphi_0^* V_y \frac{d\varphi_0}{dp_x} = 4U\varepsilon(U-\varepsilon)[(\varepsilon+U)^2 - q^2]. \qquad (28)$$

This expression is constant on the trajectory, as is $\varphi_0^*\varphi_0$, Eq. (27). Therefore, in order to find δ in Eq. (22), we have to integrate along the trajectory

$$\oint \frac{dp_x}{v_y}.$$

This integral equals $-dS(\varepsilon)/d\varepsilon$, where $S(\varepsilon) = \pi q^2$ is the cross-sectional area, Eq. (17), with

$$\frac{dS(\varepsilon)}{d\varepsilon} = \pi\varepsilon\frac{2(q^2 + U^2 - \varepsilon^2) + \gamma_1^2}{q^2 - U^2 - \varepsilon^2}. \qquad (29)$$

We now have to substitute Eqs. (27)–(29) in Eq. (22). Thus, we find the Berry phase

$$\delta(\varepsilon) = -\frac{\varepsilon U}{q^2 - \varepsilon^2 - U^2} = -\frac{\varepsilon U}{\sqrt{4U^2\varepsilon^2 + (\varepsilon^2 - U^2)\gamma_1^2}} \qquad (30)$$

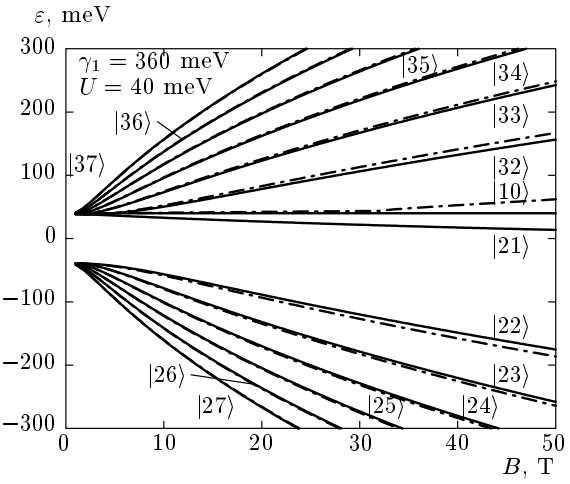

Fig. 6. Energy levels ε_{sn} for the K valley in magnetic fields for bilayer graphene within the perturbation approximation (solid lines) and in the semiclassical approach (dash-dotted lines); in the notation $|sn\rangle$, n is the Landau number and $s = 1, 2, 3, 4$ is the band number; only two nearest bands ($s = 2, 3$) are shown at given n from 0 to 7. There is only one level, $|10\rangle$, with $n = 0$ and three levels ($s = 1, 2, 3$) with $n = 1$. The levels for the K' valley can be obtained by mirror reflection with respect to the $\varepsilon = 0$ axis

shown in Fig. 5, where the δ-phase of bilayer graphene with trigonal warping is also shown; the detailed calculations will be published elsewhere. For the ungaped bilayer, $U = 0$, the Berry phase $\delta(\varepsilon) = 0$. The Berry phase depends on the energy and $\delta = \mp 1/2$ at $\varepsilon = \pm U$. At large energies, $\varepsilon \gg U$, the Berry phase $\delta \to \mp U/\gamma_1$.

Substituting Eq. (30) in the semiclassical quantization condition, Eq. (17), and solving the equation obtained for ε, we obtain the energy levels as functions of the magnetic field. We have to note that the Landau numbers n listed in Fig. 6 do not coincide with the numbers n_{sc} in semiclassical condition (17). The rigorous quantization shows that there are only one Landau level with $n = 0$ and three Landau levels with $n = 1$ [16]. These levels are not correctly described within the semiclassical approach. However, for $n \geq 2$, there are levels in all four bands s (two nearest bands with $s = 2, 3$ are shown in Fig. 6). They correspond to the semiclassical number $n_{sc} = n - 1$, and the semiclassical levels for larger n are in excellent agreement with the levels obtained in the perturbation approximation.

6. MAGNETO-OPTICS EFFECTS IN GRAPHENE LAYERS

An important peculiarity of conductivities in the presence of magnetic fields is the appearance of the Hall component $\sigma_{xy}(\omega)$. The Hall conductivity violates the rotational symmetry of graphene around the major axis. This implies rotation of the linearly polarized electromagnetic wave, i. e., the Faraday and Kerr effects for transmitted and reflected waves, correspondingly. First of all, the electron transitions are possible between the levels with the neighboring Landau numbers n and different bands s, and therefore the resonance denominators $\Delta_{ss'n} = \varepsilon_{sn} - \varepsilon_{s',n+1}$ arise in the conductivity tensor.

Calculations [16] give the conductivities for graphite in the collisionless limit when the electron collision frequency Γ is much less than the level splitting:

$$\left.\begin{matrix}\sigma_{xx}(\omega)\\ i\sigma_{xy}(\omega)\end{matrix}\right\} = i\sigma_d \frac{4\omega_B^2}{\pi^2} \sum_{n,s,s'} \int_0^{\pi/2} dz \frac{\Delta f_{ss'n}}{\Delta ss'n} |d_{ss'n}|^2 \times$$
$$\times \left[(\omega + i\Gamma + \Delta_{ss'n})^{-1} \pm (\omega + i\Gamma - \Delta_{ss'n})^{-1}\right], \quad (31)$$

where the integration is taken over the reduced Brillouin zone, $0 < z < \pi/2$. Such an integration is absent for graphene and a bilayer. Here, $\Delta f_{ss'n} = f(\varepsilon_{s'n+1}) - f(\varepsilon_{sn})$ is the difference of the Fermi functions and

$$d_{ss'n} = C^2_{sn} C^1_{s'n+1} + C^3_{sn} C^4_{s'n+1} + (\tilde{\gamma}_4/\gamma_0)(C^1_{sn} C^4_{s'n+1} + C^2_{sn} C^3_{s'n+1})$$

is the dipole matrix element expressed in terms of wave functions (9). These transitions are most intensive. They obey the selection rule

$$\Delta n = 1,$$

and are referred to as strong lines. The conductivity units

$$\sigma_d = \frac{e^2}{4\hbar d_0}$$

have the simple meaning of the graphene universal conductivity $e^2/4\hbar$ times the number $1/d_0$ of layers within the distance unit in the major axis direction.

Besides, we have to take the renormalization of the dipole moments due to trigonal warping into account. This additional electron–photon vertex results in weak lines with the selection rule

$$\Delta n = 2.$$

We obtain this contribution by substituting

$$d_{ss'n} = (\tilde{\gamma}_3/\gamma_0) C^2_{sn} C^4_{s'n+2}$$

instead of the matrix element in Eq. (31) and replacing the subscript $n + 1 \to n + 2$. We have to note

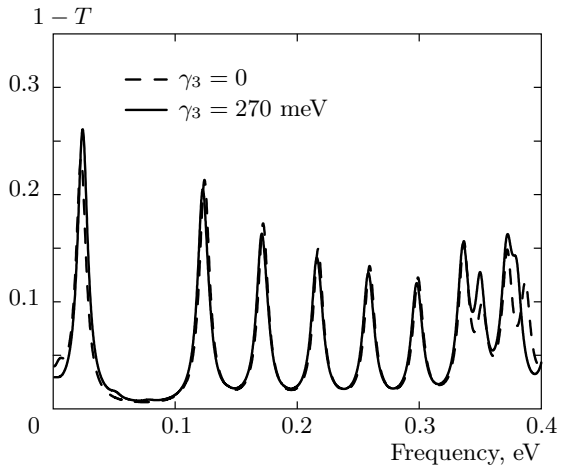

Fig. 7. Transmission spectra of gapped bilayer graphene without and with trigonal warping (dashed and solid lines, correspondingly) at $B = 10$ T and $U = 30$ meV; the band parameters used are $v = 1 \cdot 10^8$ cm/s, $\gamma_1 = 360$ meV, $\gamma_4 = -150$ meV, $\varepsilon_F = 30$ meV, and others are listed in the figure. The relaxation frequency is assumed to be $\Gamma = 5$ meV

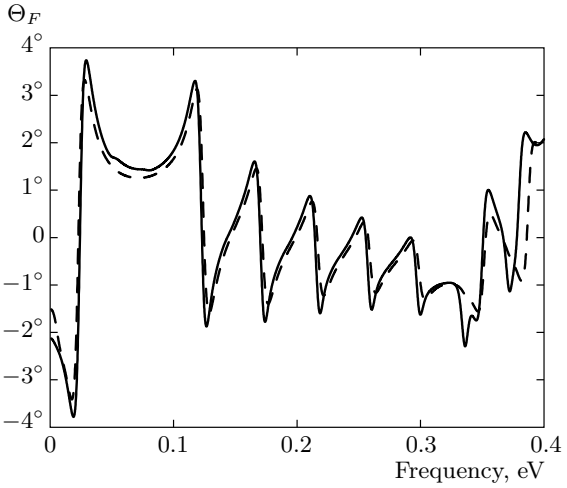

Fig. 8. Faraday rotation in gapped bilayer graphene; the parameters used are the same as in Fig. 7

that the γ_4 corrections give a linear contribution (in the small parameter γ_4/γ_0) to the conductivities at the main electron transitions with $\Delta n = 1$. The γ_3 corrections are quadratic, but they result in the appearance of new resonant transitions with $\Delta n = 2$.

There are also small so-called vertex corrections to the self-energy shown at the bottom of Fig. 4. They result from the quartet of the coupled Landau levels, which interfere while the selection rules $\Delta n = 1$ and $\Delta n = 2$ are allowed.

6.1. Gapped bilayer graphene

Graphene and bilayer graphene affect the transmission and the Faraday rotation in a linear order in the fine structure constant, whereas the reflected light intensity is quadratic in α. We therefore discuss the characteristics of light transmitted through bilayer graphene where the effects have a maximum value. In this case, Eq. (31) is valid without the integration over the z momentum component. The conductivity units should be taken now as $\sigma_0 = e^2/4\hbar$. In the approximation linear in conductivities, the transmission coefficient T and the Faraday angle for the free standing bilayer are given by

$$1 - T = \frac{4\pi}{c} \operatorname{Re} \sigma_{xx}, \quad \Theta_F = \frac{2\pi}{c} \operatorname{Re} \sigma_{xy}. \tag{32}$$

Results of calculations are shown in Figs. 7 and 8. The peaks in absorption, Fig. 7, correspond to the electron transitions. There is the series of seven lines in the 0.1–0.4 eV interval. They are doublets excited by the electron transitions of the type $|2n\rangle \to |3, n+1\rangle$ and $|3n\rangle \to |2, n+1\rangle$ for n from 2 to 8. Two weaker lines at 350 and 380 meV respectively result from the $|10\rangle \to |31\rangle$ and $|21\rangle \to |42\rangle$ transitions. There is the strongest line at 24 meV excited by the $|21\rangle \to |32\rangle$ transition. All these lines obey the selection rule $\Delta n = 1$.

The very weak lines at 51 and 78 meV owe their appearance to the $\Delta n = 2$ transitions $|21\rangle \to |33\rangle$ and $|10\rangle \to |22\rangle$.

In general, the effect of the small constants γ_3 and γ_4 is more conspicuous on the low levels $|10\rangle$ and $|21\rangle$.

The transition frequencies in the Faraday rotation, Fig. 7, are determined by the derivative of the maximum values.

6.2. Graphite

Using the conductivities in Eqs. (31), we find the complex bulk dielectric function $\varepsilon_{ij} = \delta_{ij} + 4\pi i \sigma_{ij}/\omega$ and the reflection coefficient and the Kerr rotation (see, e.g., [62]),

$$R = \frac{1}{2}(|r_+|^2 + |r_-|^2), \quad \Theta_K = \frac{1}{2} \arg(r_- r_+^*),$$

where $r_\pm = (1 - \sqrt{\varepsilon_\pm})/(1 + \sqrt{\varepsilon_\pm})$ are the reflection Fresnel coefficients for two circular polarizations with $\varepsilon_\pm = \varepsilon_{xx} \pm \varepsilon_{xy}$.

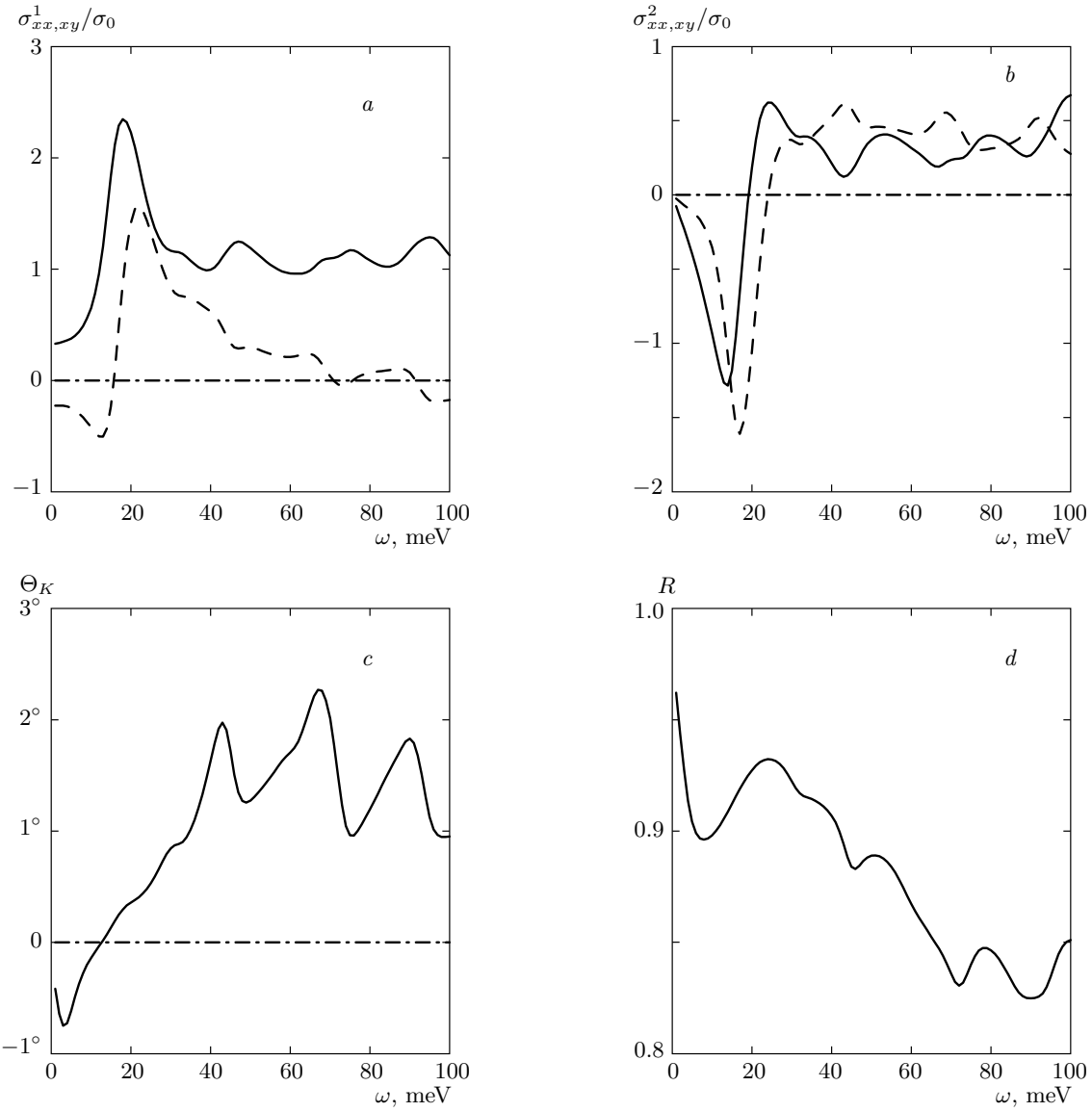

Fig. 9. (*a*) Real and (*b*) imaginary parts of the longitudinal (xx, solid line) and Hall (xy, dashed line) dynamical conductivities calculated for one graphite layer in units of $\sigma_0 = e^e/4\hbar$; (*c*) Kerr angle and (*d*) reflectivity. The magnetic field $B = 7$ T, the temperature $T = 0.1$ meV is less than the level broadening $\Gamma = 3.5$ meV

The parameters in Eq. (2) used in the calculations are listed in Table (see also Ref. [63]). The hopping integrals γ_0 to γ_3 are close to the values determined in observations of the semiclassical Shubnikov–de Haas effect. The Fermi energy equal to $\varepsilon_F = -4.1$ meV agrees at the zero magnetic field with the measurements of the extremal Fermi-surface cross sections and the masses of holes and electrons. Connections with the notation for similar parameters of the SWMC model are given in the "SWMC" line. The values of the parameters γ_4, γ_5, and Δ determined in various experiments are very different; we use γ_5 and Δ obtained by Doezema et al. [4] (given in the Table in the "SWMC" notations) and take the close value for γ_4. In the quantum limit, when electrons and holes occupy only the $|10\rangle$ and $|21\rangle$ levels, the Fermi energy must cross these close levels at the middle of the KH line. This means that the Fermi level becomes higher at such magnetic fields, taking the value $\varepsilon_F \approx -1$ meV.

The results of calculations are represented in Figs. 9, 10. We emphasize that the imaginary part of the dynamical conductivity is of the order of the real part.

It follows from Fig. 9*a* that the averaged longitudi-

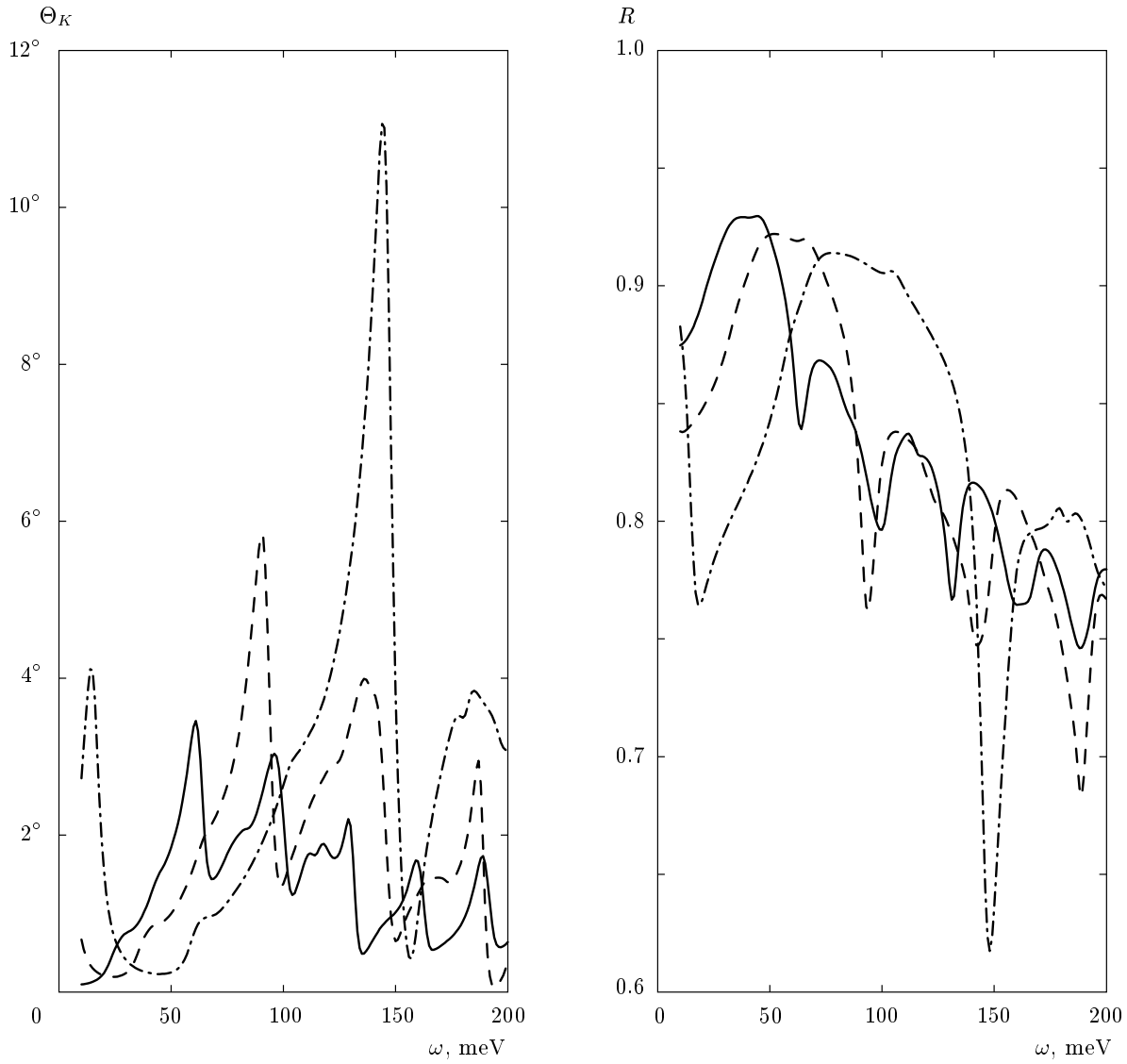

Fig. 10. Kerr angle and reflectivity at 10 (solid lines), 15 (dashed lines), and 25 T (dash-dotted lines)

nal conductivity calculated per one graphite layer tends to the graphene universal conductance. The main contribution to the sharp 16-meV line results from the electron $|21\rangle \to |32\rangle$ transition (15 meV) about the K point (see Fig. 3), where the $|32\rangle$ level coincides with the Fermi level (within an accuracy of the width Γ or temperature T). Then the transitions $|22\rangle \to |21\rangle$ produce a broad band. The low-frequency side of the band (23 meV, at the intersection of the $|21\rangle$ level with the Fermi level) contributes to the 16-meV line. In the same 16-meV line, the transitions $|32\rangle \to |33\rangle$ can contribute as well if the band $|32\rangle$ contains electrons.

The next doublet at 43 meV arises from the transitions $|23\rangle \to |32\rangle$ and $|22\rangle \to |33\rangle$ at the K point. The 68-meV doublet appears as the splitting of the $|24\rangle \to$ $\to |33\rangle$ (65 meV) and $|23\rangle \to |34\rangle$ (69 meV) transitions due to the electron–hole asymmetry at the K point of the Brillouin zone.

The 89-meV line is more complicated. First, there are the electron transitions $|24\rangle \to |35\rangle$ (89 meV) and $|25\rangle \to |34\rangle$ (90 meV) near the K point. Besides, the transitions $|11\rangle \to |10\rangle$ (95 meV) near the H point make a contribution as well. All these lines obeying the selection rule $\Delta n = 1$ are strong. There are two weak lines in the frequency range. One ($|24\rangle \to |32\rangle$) is seen at 55 meV as a shoulder on the theoretical curve. The other, at 31 meV, results from the transitions $|10\rangle \to |32\rangle$ near the K point.

The positions of the lines for fields in the range 10–30 T agree with observations in Refs. [8, 18].

The optical Hall conductivity $\sigma_{xy}(\omega)$ in the ac regime is shown in Figs. 9*a* and 9*b*. The conductivities $\sigma_{xx}(\omega)$ and $\sigma_{xy}(\omega)$ allow calculating the Kerr rotation and the reflectivity as functions of frequency (see Figs. 9*c* and 9*d*). It is evident that the interpretation of the Kerr rotation governed by the conductivity $\sigma_{xy}(\omega)$ is much more complicated in comparison with the longitudinal conductivity. The Kerr angle and reflectivity shown in Fig. 10 for the different magnetic fields demonstrate a strong field dependence of the magneto-optic phenomena.

7. SUMMARY AND CONCLUSIONS

We have evaluated the perturbation theory for the matrix Hamiltonian, which permits calculating the corrections to eigenvalues resulting from the small matrix elements, particularly from the trigonal warping. The trigonal warping in graphite can be considered within the perturbation theory at strong magnetic fields larger than approximately 1 T. For weak magnetic fields, when the Fermi energy is much larger than the cyclotron frequency, the semiclassical quantization with the Berry phase included can be applied. We have found that the principal electron transitions obey the selection rule $\Delta n = 1$ for the Landau number n, but the $\Delta n = 2$ transitions due to the trigonal warping with a small probability are also essential. In graphite, the electron transitions at the K and H points as well as at intersections of the Landau levels with the Fermi level make contributions to conductivity. The good agreement between the calculations and the measured Kerr rotation and reflectivity in graphite in the quantizing magnetic fields is achieved. The SWMC parameters are used in the fit taking their values from the previous de Haas–van Alphen measurements and increasing the Fermi energy value in the case of strong magnetic fields.

We acknowledge the useful discussions with A. Kuzmenko and J. Levallois. This work was supported by the RFBR (grant No. 10-02-00193-a) and the SCOPES (grant IZ73Z0_128026).

REFERENCES

1. J. C. Slonchewski and P. R. Weiss, Phys. Rev. **109**, 272 (1958); J. W. McClure, Phys. Rev. **108**, 612 (1957).
2. H. Suematsu and S.-I. Tanuma, J. Phys. Soc. Jpn. **33**, 1619 (1972).
3. W. W. Toy, M. S. Dresselhaus, and G. Dresselhaus, Phys. Rev. B **15**, 4077 (1977).
4. R. E. Doezema, W. R. Datars, H. Schaber, and A. Van Schyndel, Phys. Rev. B **19**, 4224 (1979).
5. E. Mendez, A. Misu, and M. S. Dresselhaus, Phys. Rev. B **21**, 827 (1980).
6. Z. Q. Li, S.-W. Tsai, W. J. Padilla et al., Phys. Rev. B **74**, 195404 (2006).
7. M. Orlita, C. Faugeras, G. Martinez et al., Phys. Rev. Lett. **100**, 136403 (2008).
8. M. Orlita, C. Faugeras, J. M. Schneider et al., Phys. Rev. Lett. **102**, 166401 (2009).
9. M. Orlita and M. Potemski, Semicond. Sci. Technol. **25**, 063001 (2010).
10. I. Crassee, J. Levallois, A. L. Walter et al., Nature Phys. **7**, 48 (2011).
11. Y. Kopelevich, J. H. S. Torres, R. R. da Silva et al., Phys. Rev. Lett. **90**, 156402 (2003).
12. I. A. Luk'yanchuk and Y. Kopelevich, Phys. Rev. Lett. **97**, 256801 (2006).
13. Z. Jiang, Y. Zhang, H. L. Stormer, and P. Kim, Phys. Rev. Lett. **99**, 106802 (2007).
14. J. M. Schneider, M. Orlita, M. Potemski, and D. K. Maude, Phys. Rev. Lett. **102**, 166403 (2009).
15. A. N. Ramanayaka and R. G. Mani, Phys. Rev. B **82**, 165327 (2010).
16. L. A. Falkovsky Phys. Rev. B **84**, 115414 (2011).
17. G. Li and E. Y. Andrei, Nature Phys. **3**, 623 (2007).
18. K.-C. Chuang, A. M. R. Baker, and R. J. Nicholas, Phys. Rev. B **80**, 161410(R) (2009).
19. L. M. Zhang, Z. Q. Li, D. N. Basov et al., Phys. Rev. B **78**, 235408 (2008).
20. H. Ushio, T. Uda, and Y. Uemura, J. Phys. Soc. Jpn. **33**, 1551 (1972).
21. K. Nakao, J. Phys. Soc. Jpn. **40**, 761 (1976).
22. B. Partoens and F. M. Peeters, Phys. Rev. B **74**, 075404 (2006).
23. A. Grüneis, C. Attaccalite, L. Wirtz et al., Phys. Rev. B **78**, 205425 (2008).
24. A. B. Kuzmenko, I. Crassee, D. van der Marel et al., Phys. Rev. B **80**, 165406 (2009).

25. L. A. Falkovsky, Zh. Eksp. Teor. Fiz. **49**, 609 (1965).

26. G. Dresselhaus, Phys. Rev. B **10**, 3602 (1974).

27. D. C. Elias, R. V. Gorbachev, A. S. Mayorov et al., Nature Phys. **7**, 701 (2011).

28. A. A. Abrikosov and S. D. Beneslavsky, Zh. Eksp. Teor. Fiz. **59**, 1280 (1970).

29. J. Gonzalez, F. Guinea, and M. A. H. Vozmediano, Nucl. Phys. B **424**, 595 (1994); J. Gonzalez, F. Guinea, and M. A. H. Vozmediano, Phys. Rev. B **59**, 2474 (1999).

30. E. G. Mishchenko, Phys. Rev. Lett. **98**, 216801 (2007).

31. E. McCann and V. I. Fal'ko, Phys. Rev. Lett. **96**, 086805 (2006).

32. C. L. Lu, C. P. Chang, Y. C. Huang et al., Phys. Rev. B **73**, 144427 (2006).

33. T. Ohta, A. Bostwick, T. Seyller et al., Science **313**, 951 (2006).

34. L. M. Zhang, Z. Q. Li, D. N. Basov et al., Phys. Rev. B **78**, 235408 (2008).

35. A. B. Kuzmenko, E. van Heumen, D. van der Marel et al., Phys. Rev. B **79**, 115441 (2009).

36. Z. Q. Li, E. A. Henriksen, Z. Jiang et al., Phys. Rev. Lett. **102**, 037403 (2009).

37. E. V. Castro, K. S. Novoselov, S. V. Morozov et al., Phys. Rev. Lett. **99**, 216802 (2007).

38. E. J. Nicol and J. P. Carbotte, Phys. Rev. B **77**, 155409 (2008).

39. K. F. Mak, C. H. Lui, J. Shan, and T. F. Heinz, Phys. Rev. Lett. **102**, 256405 (2009).

40. A. B. Kuzmenko, I. Crassee, D. van der Marel et al., arXiv:0908.0672.

41. J. C. Charlier, X. Gonze, and J. P. Michenaud, Phys. Rev. B **43**, 4579 (1982).

42. L. A. Falkovsky and A. A. Varlamov, arXiv:cond-mat/0606800; Eur. Phys. J. B **56**, 281 (2007).

43. V. P. Gusynin, S. G. Sharapov, and J. P. Carbotte, Phys. Rev. B **75**, 165407 (2007); arXiv: cond-mat/0607727, Phys. Rev. Lett. **96**, 256802 (2006).

44. L. A. Falkovsky, Phys. Rev. B **75**, 033409 (2007).

45. L. A. Falkovsky and S. S. Pershoguba, Phys. Rev. B **76**, 153410 (2007).

46. R. R. Nair, P. Blake, A. N. Grigorenko et al., Science **320**, 5881 (2008).

47. Z. Q. Li, E. A. Henriksen, Z. Jiang et al., Nature Phys. **4**, 532 (2008).

48. K. F. Mak, M. Y. Sfeir, Y. Wu et al., Phys. Rev. Lett. **101**, 196405 (2008).

49. A. B. Kuzmenko, E. van Heumen, F. Carbote, and D. van der Marel, Phys. Rev. Lett. **100**, 117401 (2008).

50. L. A. Falkovsky, Phys. Rev. B **82**, 073103 (2010).

51. A. K. Geim and K. S. Novoselov, Nature Mater. **6**, 183 (2007).

52. A. H. Castro Neto, F. Guinea, N. M. R. Peres, and K. S. Novoselov, Rev. Mod. Phys. **81**, 109 (2009).

53. M. V. Berry, Proc. Roy. Soc. London A **392**, 45 (1984).

54. G. P. Mikitik and Yu. V. Sharlai, Zh. Eksp. Teor. Fiz. **114**, 1375 (1998); Phys. Rev. B **67**, 115114 (2003).

55. P. Carmier and D. Ullmo, Phys. Rev. B **77**, 245413 (2008).

56. A. A. Taskin and Y. Ando, Phys. Rev. B **84**, 035301 (20011).

57. E. V. Kurganova, H. J. van Eleferen, A. McCollam et al., Phys. Rev. B **84**, 121407 (20011).

58. Cheol-Hwan Park and N. Marzari, Phys. Rev. B **84**, 205440 (2011).

59. Singhun Park and H.-S. Sim, Phys. Rev. B **84**, 235432 (2011).

60. Y. Liu, G. Bian, T. Miller, and T.-C. Chiang, Phys. Rev. Lett. **107**, 166803 (2011).

61. L. M. Zhang, M. M. Fogel, and D. P. Arovas, Phys. Rev. B **84**, 075451 (2011).

62. J. Levallois, M. Tran, and A. B. Kuzmenko, arXiv: 1110/2754v2.

63. N. B. Brandt, S. M. Chudinov, and Ya. G. Ponomarev, *Semimetals* I. *Graphite and its Compounds*, Elsevier, Amsterdam (1988).